PAPER

Non-magnetic ion site disorder effects on the quantum magnetism of a spin-1/2 equilateral triangular lattice antiferromagnet

IOP Publishing Journal of Physics: Condensed Matter
J. Phys.: Condens. Matter **34** (2022) 205401 (10pp) https://doi.org/10.1088/1361-648X/ac5703

Non-magnetic ion site disorder effects on the quantum magnetism of a spin-1/2 equilateral triangular lattice antiferromagnet

Q Huang[1,*], R Rawl[1], W W Xie[2], E S Chou[3], V S Zapf[4], X X Ding[4], C Mauws[5], C R Wiebe[5,6,7], E X Feng[8], H B Cao[8], W Tian[8], J Ma[9,10], Y Qiu[11], N Butch[11] and H D Zhou[1,3]

[1] Department of Physics and Astronomy, University of Tennessee, Knoxville, TN 37996, United States of America
[2] Department of Chemistry and Chemical Biology, Rutgers University, Piscataway, NJ 08854, United States of America
[3] National High Magnetic Field Laboratory, Florida State University, Tallahassee, FL 32310, United States of America
[4] National High Magnetic Field Laboratory, Los Alamos National Laboratory, Los Alamos, NM 87545, United States of America
[5] Department of Chemistry, University of Manitoba, Winnipeg, Manitoba R3T 2N2, Canada
[6] Department of Chemistry, University of Winnipeg, Winnipeg, Manitoba R3B 2E9, Canada
[7] Department of Physics and Astronomy, McMaster University, Hamilton, Ontario L8S 4M1, Canada
[8] Neutron Scattering Division, Oak Ridge National Laboratory, Oak Ridge, TN 37831, United States of America
[9] Laboratory of Artificial Structures and Quantum Control, School of Physics and Astronomy, Shanghai Jiao Tong University, Shanghai 200240, People's Republic of China
[10] Shenyang National Laboratory for Materials Science, Institute of Metal Research, Chinese Academy of Sciences, 110016 Shenyang, People's Republic of China
[11] NIST Center for Neutron Research, National Institute of Standards and Technology, Gaithersburg, MD 20899, United States of America

E-mail: qhuang11@vols.utk.edu

Received 6 December 2021, revised 12 January 2022
Accepted for publication 21 February 2022
Published 10 March 2022

Abstract

With the motivation to study how non-magnetic ion site disorder affects the quantum magnetism of $Ba_3CoSb_2O_9$, a spin-1/2 equilateral triangular lattice antiferromagnet, we performed DC and AC susceptibility, specific heat, elastic and inelastic neutron scattering measurements on single crystalline samples of $Ba_{2.87}Sr_{0.13}CoSb_2O_9$ with Sr doping on non-magnetic Ba^{2+} ion sites. The results show that $Ba_{2.87}Sr_{0.13}CoSb_2O_9$ exhibits (i) a two-step magnetic transition at 2.7 K and 3.3 K, respectively; (ii) a possible canted 120 degree spin structure at zero field with reduced ordered moment as 1.24 μ_B/Co; (iii) a series of spin state transitions for both $H \parallel ab$-plane and $H \parallel c$-axis. For $H \parallel ab$-plane, the magnetization plateau feature related to the up–up–down phase is significantly suppressed; (iv) an inelastic neutron scattering spectrum with only one gapped mode at zero field, which splits to one gapless and one gapped mode at 9 T. All these features are distinctly different from those observed for the parent compound $Ba_3CoSb_2O_9$, which demonstrates that the non-magnetic ion site disorder (the Sr doping) plays a complex role on the magnetic properties beyond the conventionally expected randomization of the exchange interactions. We propose the additional effects including the enhancement of quantum spin fluctuations and introduction of a possible spatial anisotropy through the local structural distortions.

* Author to whom any correspondence should be addressed.

Keywords: geometrically frustrated magnet, site disorder, phase transitions

(Some figures may appear in colour only in the online journal)

1. Introduction

Quantum magnets are the focus of modern condensed matter physics research, since they not only provide unique opportunities to explore quantum many-body physics but also have potential applications in advanced technologies such as spintronics and quantum computers. More attention has recently been paid to their disorder effects, since materials inevitably have defects and/or random disorder. Compared to the disorder on magnetic ion sites which usually destroys the magnetic interactions and leads to glassy or paramagnetic states, the disorder on non-magnetic ion sites remains more intriguing and illusive. How such kind of disorder affects the magnetism on the chemically ordered magnetic sublattice is a challenging question with limited knowledge so far.

A good example of non-magnetic ion site disorder is the heavily studied $YbMgGaO_4$ (YMGO). In YMGO, the Yb^{3+} ions with effective spin-1/2 form a geometrically frustrated triangular layer [1, 2], between these layers the site mixture of Mg^{2+}/Ga^{3+} ions cause the intrinsic disorder of the non-magnetic ion sites. Earlier studies on YMGO show that: its inelastic neutron scattering (INS) spectrum has a continuum mode [3–6], the specific heat behaves as $C_p \sim T^{0.7}$ [1], its muon spin relaxation rate exhibits a temperature-independent plateau [7], and its DC susceptibility saturates below 0.1 ∼ 0.2 K [8]. All of which suggest that YMGO has a gapless quantum spin liquid (QSL) state. More recently, the reports including no residual κ_0/T term on the thermal conductivity observed [9] and the frequency dependent AC susceptibility peak [10], suggest a glassy ground state in YMGO which could be due to the Mg^{2+}/Ga^{3+} site disorder [2, 11]. Several theoretical models which include this site disorder effect have been proposed for YMGO: highly anisotropic nearest-neighbor interactions [12], the random singlet (RS) state [13, 14], randomness-induced QSL state [15], the mimicry of a spin liquid [16, 17], and randomness induced spin-liquid-like phase in J_1–J_2 model [18–24]. Of these, the RS state and randomness-induced QSL have also been applied to other quantum magnets with disorder [25–43]. However, a most recent study on high quality YMGO single crystals reveals a residual κ_0/T term and series of quantum spin state transitions at the zero temperature limit. This suggests the survival of itinerant excitations and quantum spin state transitions in YMGO [44].

The controversial magnetic ground state of YMGO reflects of the complex role that the disorder on the non-magnetic ion sites plays in quantum magnets. To better understand this role, more studies on quantum magnets with such kind of disorder is highly desirable. While searching for ideal quantum magnets to incorporate non-magnetic ion site disorder, $Ba_3CoSb_2O_9$ (BCSO) caught our attention. $Ba_3CoSb_2O_9$ (BCSO) is a rare example of an equilateral triangular lattice antiferromagnet (TLAF) with effective spin-1/2 (for Co^{2+} ions) and easy plane anisotropy. Its exotic quantum magnetism has been well documented. First, the theoretical studies have proposed that in a spin-1/2 TLAF, the quantum spin fluctuations stabilize a novel up–up–down (UUD) phase while approaching zero temperature with the applied field parallel to either easy plane or easy axis [45, 46]. The UUD phase exhibits itself as a magnetization plateau within a certain magnetic field regime and with one-third of the saturation moment ($1/3M_s$). Experimentally, such an UUD phase has been reported for BCSO [47–52]. Detailed studies further reveal a series of quantum spin state transitions (QSSTs) in BCSO. With increasing field along the *ab* plane, its 120 degree spin structure at zero field is followed by a canted 120 degree spin structure, the UUD phase, a coplanar phase (the V phase), and another coplanar phase (the V′ phase) before entering the fully polarized state [53–59]. While for $H \parallel c$-axis, the 120 degree spin structure will be followed by an umbrella spin structure, and the V phase. Second, several abnormal features about its spin dynamics have been experimentally studied by the INS experiments [60–64] and theoretically investigated [65–67], including the quantum renormalization of excitation energies, a rotonlike minimum at the *M* point, and the intense continuum mode extending to a high energy.

Another fact is that the triple perovskite structure for BCSO is very flexible on its chemical composition. For example, one can replace Ba^{2+} ions with Sr^{2+} or Ca^{2+} ions [68, 69], or replace Sb^{5+} ions with Nb^{5+} or Ta^{5+} ions [70–72] while keeping the Co-triangular lattice. In fact, $Ba_3CoNb_2O_9$ [70] exhibits a two-step ordering process at 1.36 K and 1.10 K with

Table 1. Data of crystallographic refinement for Sr-BCSO at 296(2) K

Crystal system	Hexagonal
F.W. (g/mol)	851.74
Space group; *Z*	$P6_3/mmc$; 2
a (Å)	5.847(3)
c (Å)	14.507(6)
V (Å^3)	429.5(4)
Extinction coefficient	0.000 44(7)
θ range (deg)	2.808–34.487
No. reflections; R_{int}	8552; 0.0254
No. independent reflections	394
No. parameters	24
R_1: ωR_2 ($I < 2\delta(I)$)	0.0104; 0.0190
Goodness of fit	1.199
Diffraction peak and hole (e$^-$/Å^3)	0.804; −0.800

Table 2. Atomic coordinates and equivalent isotropic displacement parameters of Sr-BCSO system. $U_(\,$eq) is defined as one-third of the trace of the orthogonalized $U_(\,ij)$ tensor (Å^2)

Atom	Site	Occ.	x	y	z	$U_(\,$eq)
Ba/Sr1	2b	0.952(5)/0.048	0	0	0.25	0.009(1)
Ba/Sr2	4f	0.955(4)/0.045	1/3	2/3	0.0101(1)	
Sb	4f	1	1/3	2/3	0.65183(2)	0.0066(1)
Co	2a	1	0	0	0	0.0057(1)
O1	6h	1	0.5189(2)	0.0378(2)	0.25	0.0094(4)
O2	12k	1	0.8299(2)	0.6597(3)	0.0848(1)	0.0150(3)

easy axis anisotropy and also exhibits the QSSTs. Unfortunately, so far, no single crystalline form of $Ba_3CoNb_2O_9$ has been prepared, which limits its studies.

These two features, exotic quantum magnetism and flexible chemical composition, make BCSO an ideal system to incorporate the non-magnetic ion site disorder and thereafter study its effects on quantum magnetism. In this paper, we successfully grew single crystals of $Ba_{2.87}Sr_{0.13}CoSb_2O_9$ to introduce the disorder (the mixture of Ba/Sr ions) on the non-magnetic Ba^{2+} ion sites and studied its magnetic properties by performing DC and AC susceptibility, specific heat, elastic and inelastic neutron scattering measurements. By comparing the obtained results to those of the parent compound BCSO, we learned that such disorder on the non-magnetic ion sites significantly tunes the magnetic ground state, phase diagram, and spin dynamics of this spin-1/2 equilateral TLAF.

2. Experimental

Single crystalline Sr-doped $Ba_3CoSb_2O_9$ (Sr-BCSO) was synthesized by the floating-zone method. The feed and seed rods for the crystal growth were made by solid state reaction. The appropriate amount of $BaCO_3$, $SrCO_3$, $CoCO_3$ and Sb_2O_3 were ground together, pressed into a 6 mm-diameter 10 cm-long rod under 40 MPa hydrostatic pressure, and annealed in air at 1300 °C for 20 h. The single crystal growth was carried out in a 10%O_2/90%Ar forming gas with a 0.4 MPa in an IR-heated image furnace equipped with two halogen lamps. The crystal growth rate is 30 mm/hour. The Laue back diffraction technique is used to align the single crystal sample in specific orientation for measurements. The single crystal x-ray diffraction measurement was performed in Bruker D8 Quest Eco diffractometer with Mo radiation (λK_α = 0.710 73 Å), which is equipped with photon II detector. The crystal structure, especially the atomic mixture and disorders, were refined using SHELXTL package with full matrix least-squares on F^2 model [73].

The DC magnetic susceptibility measurements were performed using a vibrating sample magnetometer option in a commercial physical property measurement system (PPMS, Quantum Design). The specific heat data was also obtained using a PPMS. The magnetization up to 35 T was measured with a vibrating sample magnetometer (VSM) at the National High Magnetic Field Laboratory (NHMFL), Tallahassee. Another magnetization measurement up to 40 T

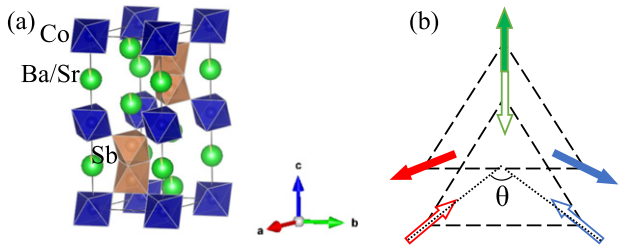

Figure 1. (a) An illustration of the crystallographic structure of Sr-BCSO. (b) An illustration of the canted 120-degree spin structure.

using compensated induction coil with sample-in/sample-out background subtraction was performed at the NHMFL, Los Alamos. The single crystal neutron diffraction measurements were performed at the High Flux Isotope Reactor (HFIR) of the Oak Ridge National Laboratory (ORNL). The zero field measurements were carried out at 300 mK with the wavelength of $\lambda = 1.5424$ Å in the Oxford cryogen-free HelioxVT refrigerator at the single crystal diffractometer DEMAND [74], HB3A and at 1.5 K with the wavelength of $\lambda = 4.2636$ Å in the orange cryostat on the Cold Neutron Triple-Axis Spectrometer, CTAX. The measurements under magnetic field were conducted at 1.5 K with the wavelength of $\lambda = 2.3779$ Å in an 8 T vertical asymmetric field cryomagnet on the Fixed-Incident-Energy Triple-Axis Spectrometer, HB1A. The diffraction patterns were analyzed by the Rietveld refinement program FullProf. The magnetic structure compatible with the lattice symmetry was obtained by SARAH software. The INS measurements under zero field were performed at 300 mK on the disk chopper spectrometer with the He-3 dipper insert in the NIST Center for Neutron Research (NCNR). The INS measurements under applied magnetic field were conducted at 1.6 K in an 11 T magnet on the multi axis crystal spectrometer (MACS) in NCNR [75].

3. Results

3.1. Crystal and magnetic structure

The refinement of the single crystal x-ray data confirms that the composition for the as-grown crystal is $Ba_{2.87}Sr_{0.13}CoSb_2O_9$. It has a hexagonal structure with the space group $P6_3/mmc$ and lattice parameters $a = 5.847(3)$ Å and $c = 14.507(6)$ Å. The detailed refinement and crystallographic information is listed

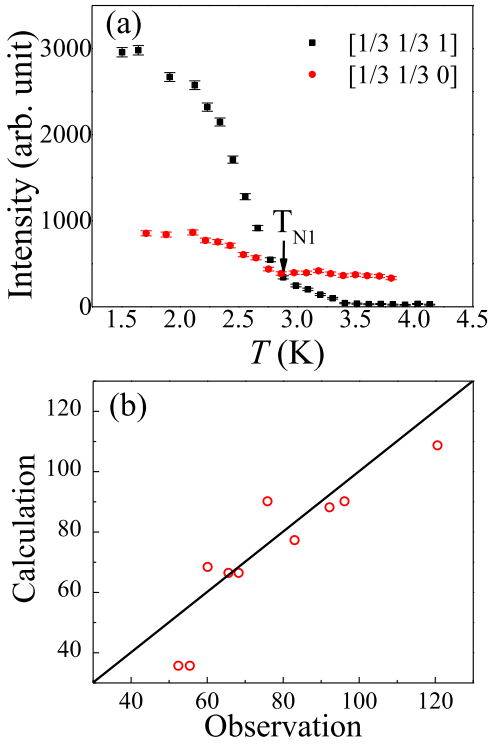

Figure 2. (a) The temperature dependence of the intensity for a magnetic peak [1/3 1/3 1] and [1/3 1/3 0]. The intensity of [1/3 1/3 0] is multiplied by a factor 20 for the visibility. Error bars represent one standard deviation. (b) The refinement result of the single crystal neutron diffraction data with a canted 120-degree spin structure. The x and y coordinates represent the observed and calculated intensities of magnetic peaks, respectively. The black guideline represents the function $x = y$.

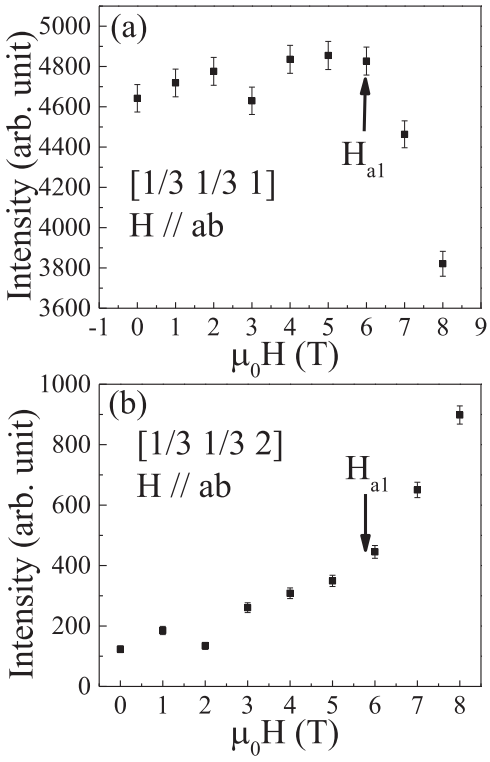

Figure 3. The field dependence of the intensity for magnetic peak [1/3 1/3 1] (a) and [1/3 1/3 2] (b) measured at 1.5 K. Error bars represent one standard deviation.

in tables 1 and 2. The results show $\sim 4\%$ Sr mixed on Ba site. Moreover, no atomic vacancies were observed on Co, Sb and O sites. As shown in figure 1(a), in this structure, each Co^{2+} ion is surrounded by six O^{2-} ions, forming a CoO_6 octahedron. The layers of the triangular lattice of CoO_6 octahedra in the *ab* plane are separated by two face-shared SbO_6 octahedra. The intralayer and interlayer distances between the Co^{2+} ions are 5.847(3) Å and 7.253(5) Å, respectively, which results in a quasi-2D triangular lattice system.

Elastic neutron scattering measurements under zero and varying applied magnetic fields were performed to probe the magnetic structure of Sr-BCSO. As shown in figure 2(a), the temperature dependence of the intensity for a magnetic peak [1/3 1/3 1] measured at zero field shows a rapid increase below $T_{N1} = 2.8$ K, which indicates a magnetic ordering. Moreover, a set of magnetic peaks indexed by propagation vector [1/3 1/3 1] were collected in a single crystal neutron scattering measurement. As shown in figure 2(b), the data can be fitted by a 120 degree spin structure in the *ab* plane. The refined magnetic moment is 1.24(7) μ_B/Co. Meanwhile, a weak intensity at zero field for the magnetic peak [1/3 1/3 0] below T_{N1} was also observed, as shown in figure 2(a). The existence of vector [1/3 1/3 0] suggests that spins in the *ab* plane should have a weak ferromagnetic moment. One possible scenario is the canted 120 degree spin structure, in which the sum of the magnetic moments of the three sublattice spins is nonzero but lead to a resultant magnetic moment, as shown in figure 1(b). Unfortunately, the exact spin structure cannot be solved due to the limited data resolution we obtained. Therefore, while the data suggests a canted spin structure as the ground state for Sr-BCSO, we still use the 120 degree spin structure to obtain the ordered moment.

The field dependence of the intensities for the [1/3 1/3 1] and [1/3 1/3 2] peaks measured at 1.5 K are shown in figures 3(a) and (b), respectively. For the [1/3 1/3 1] peak, its intensity is basically a constant from 0 T to 6 T, and then shows a drastic drop around $\mu_0 H_{a1} = 6$ T. For the [1/3 1/3 2] peak, its intensity increases with increasing field but with a slope change around 6 T. These features suggest there is a spin state transition around H_{a1}.

3.2. DC and AC magnetic susceptibility

The temperature dependence of the DC magnetic susceptibility, $\chi(T)$, under magnetic fields is shown in figure 4. As $H \parallel ab$-plane is increased (figures 4(a)–(c)), $\chi(T)$ shows several features. (i) A broad peak appears around 6 K with $\mu_0 H < 5$ T; (ii) a peak appears around 3 K at $\mu_0 H = 5$ T, which is labeled as T_{N1} and shifts to lower temperatures with increasing field; (iii) in addition to the peak at T_{N1}, at $\mu_0 H = 7$ T the data shows that $\chi(T)$ increases rapidly below 5 K. Here we use the peak position of its second-order derivative (figure 4(c)) to represent this feature, labeled as T_{N2}. With increasing field, T_{N2} shifts to higher temperatures between 7 T $\leqslant \mu_0 H \leqslant$ 11 T; (iv) with $\mu_0 H \geqslant 12$ T, the feature at T_{N2} involves to be a peak again (figure 4(b)).

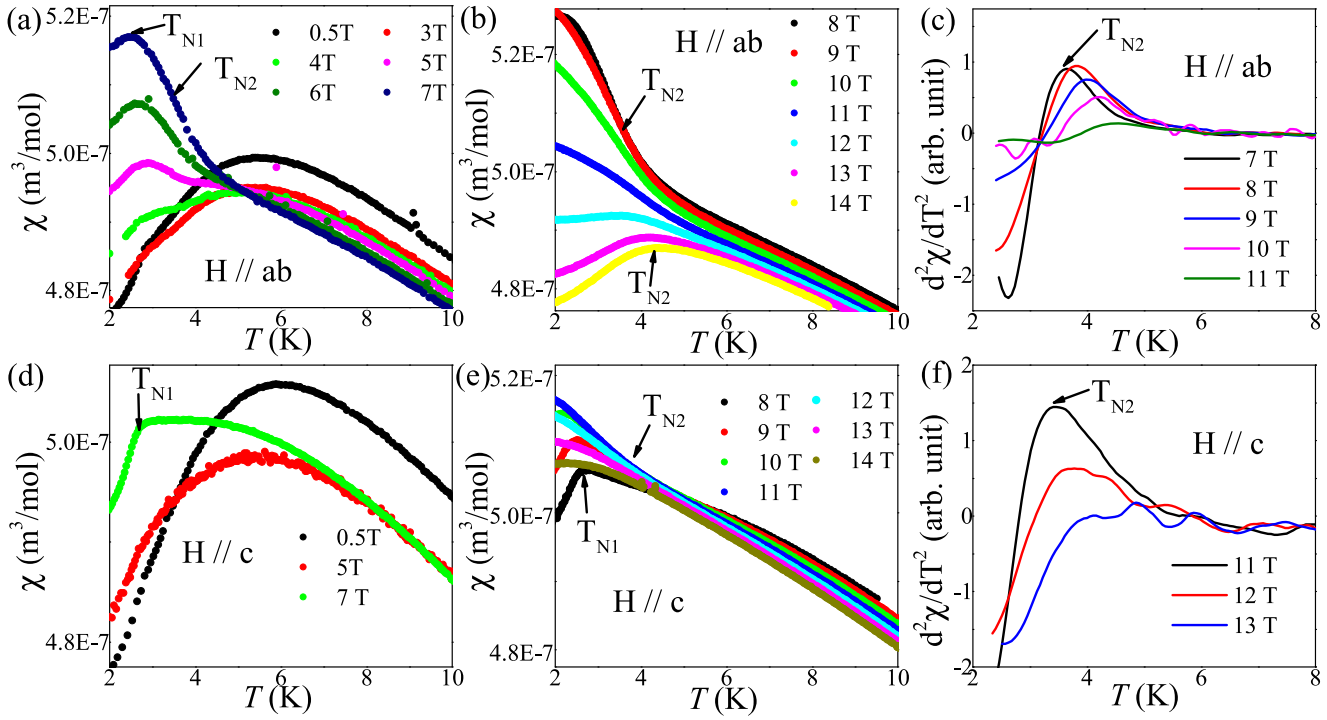

Figure 4. The temperature dependence of the DC susceptibility under different magnetic fields with $H \parallel ab$-plane (a) and (b) and $H \parallel c$-axis (d) and (e) for Sr-BCSO. The second-order derivative of the χ–T curves under high magnetic fields for $H \parallel ab$-plane (c) and $H \parallel c$-axis (f).

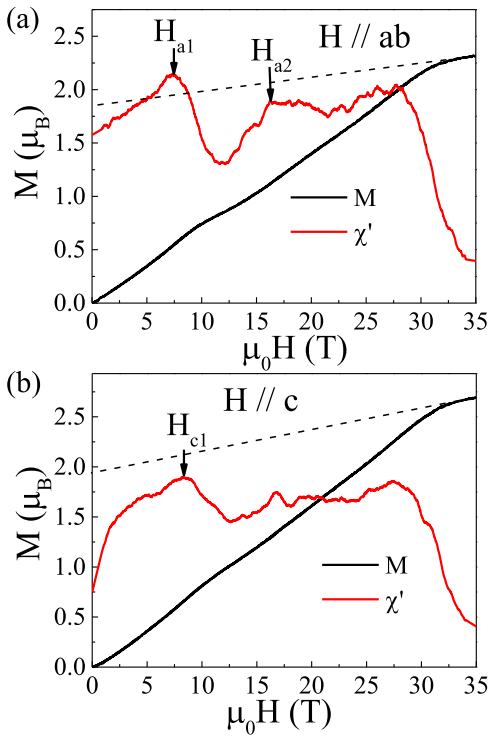

Figure 5. The dc magnetization (black line) and its derivative (red line) measured at 1.5 K with $H \parallel ab$-plane (a) and $H \parallel c$-axis (b). The dashed line represents the Van Vleck paramagnetic background.

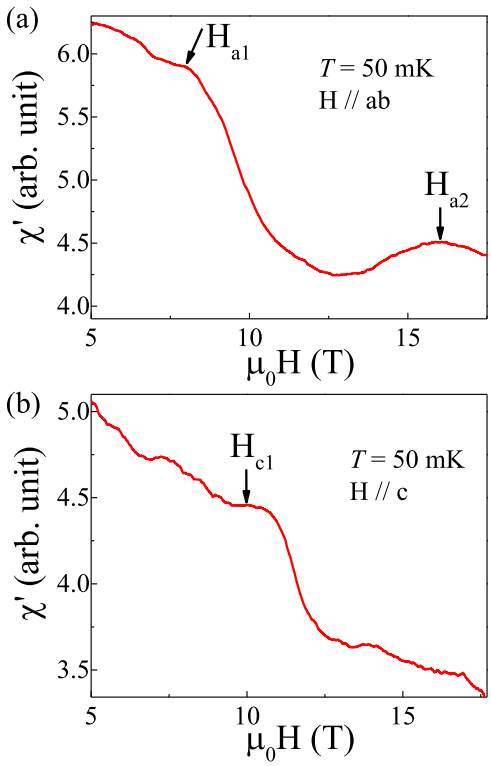

Figure 6. The AC susceptibility measured at 50 mK with $H \parallel ab$-plane (a) and c-axis (b).

For $H \parallel c$-axis, the peak at T_{N1} is not as strong as that for $H \parallel ab$-plane and appears when $\mu_0 H \geqslant 7$ T (figure 4(d)). The feature at T_{N2} also appears when $\mu_0 H > 11$ T (figures 4(e) and (f)). Compared to the $H \parallel ab$-plane case, for the $H \parallel c$-axis, both features appear at a higher magnetic field.

As shown in figure 5, the DC magnetization, $M(H)$, measured at 1.5 K by using a VSM shows a weak plateau feature

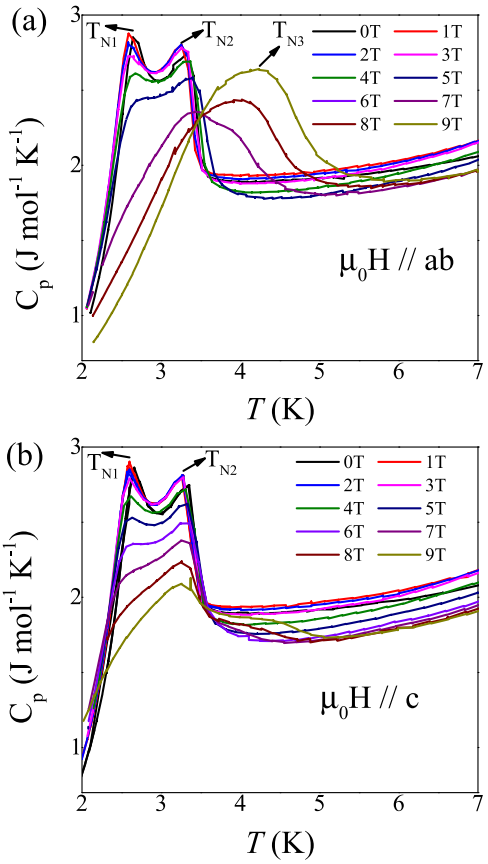

Figure 7. The temperature dependence of specific heat measured with $H \parallel ab$-plane (a) and $H \parallel c$-axis (b).

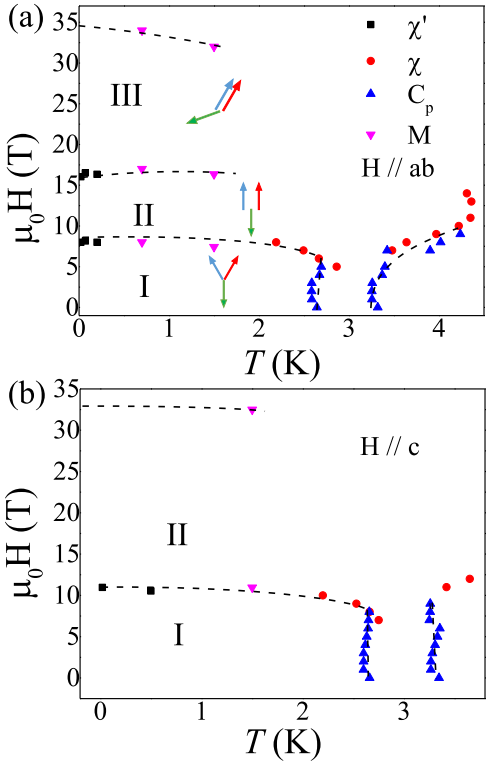

Figure 8. The magnetic phase diagram for $H \parallel ab$-plane (a) and $H \parallel c$-axis (b).

for $H \parallel ab$-plane while only a slope change for $H \parallel c$-axis. Accordingly, the derivative dM/dH for $H \parallel ab$-plane shows a peak-valley-peak feature with two critical fields $\mu_0 H_{a1} = 7.5$ T and $\mu_0 H_{a2} = 16.4$ T. Meanwhile, the derivative for $H \parallel c$-axis only shows one peak at $\mu_0 H_{c1} = 8.7$ T. The saturation field is around 33 T for both directions. The saturation moments are 1.8 μ_B/Co and 1.9 μ_B/Co for $H \parallel ab$-plane and $H \parallel c$-axis, respectively. For $H \parallel ab$-plane, the DC magnetization was also measured at 0.7 K by using a compensated induction coil with sample-in/sample-out background subtraction (not shown here), which shows similar behavior to the 1.5 K data.

Since the field dependent AC magnetic susceptibility, $\chi'(H)$, is basically equivalent to dM/dH, we measured $\chi'(H)$ at 50 mK to double check the critical fields. As shown in figure 6, two critical fields at $\mu_0 H_{a1} = 8.1$ T and $\mu_0 H_{a2} = 16.0$ T for $H \parallel ab$-plane and one at $\mu_0 H_{c1} = 9.8$ T for $H \parallel c$-axis were observed. This is consistent with the DC $M(H)$ results. Since the $\chi'(H)$ signal is on top of the coil background, it appears less pronounced than dM/dH in figure 5.

3.3. Specific heat

Figure 7 shows the temperature dependence of the specific heat, C_p, measured at different fields. At zero field, C_p shows two sharp peaks at $T_{N1} = 2.7$ K and $T_{N2} = 3.3$ K, respectively, which indicates a two-step magnetic ordering. The T_{N1} value is consistent with the ones determined by the neutron diffraction and $\chi(T)$ data. With increasing field $H \parallel ab$-plane, these two peaks at T_{N1} and T_{N2} become less pronounced while their positions remain almost unchanged. The peak at T_{N1} disappears around 6.5 T while the peak at T_{N2} disappears around 8 T. At around 7 T, another broad peak start to appear, labeled as T_{N3} (figure 7(a)). This peak becomes stronger and shifts to higher temperatures with increasing field. For $H \parallel c$-axis (figure 7(b)), the peak at T_{N1} becomes weaker with increasing field and is unrecognizable around 8 T. Meanwhile, the peak at T_{N2} does not change obviously. Apparently, the evolution of C_p under field is quite different between the $H \parallel ab$-plane and $H \parallel c$-axis cases.

3.4. Magnetic phase diagrams

Magnetic phase diagrams for $H \parallel ab$-plane and $H \parallel c$-axis were constructed by using the critical temperatures and fields obtained above, as shown in figure 8. Besides the high temperature paramagnetic phase and high field fully polarized phase, the $H \parallel ab$-plane phase diagram includes three phases while the $H \parallel c$-axis one has two phases.

3.5. Inelastic neutron scattering spectra

The INS spectra of Sr-BCSO were measured at zero field and 9 T in the *ab* plane, which allows us to study the spin dynamics in phase I and II in figure 8(a). Figures 9(a) and (b) show the INS spectra dispersion up to ∼2.5 meV along the [H H 1] and [1/3 1/3 L] directions at zero field, respectively. While the intralayer dispersion is sharp and the interlayer dispersion

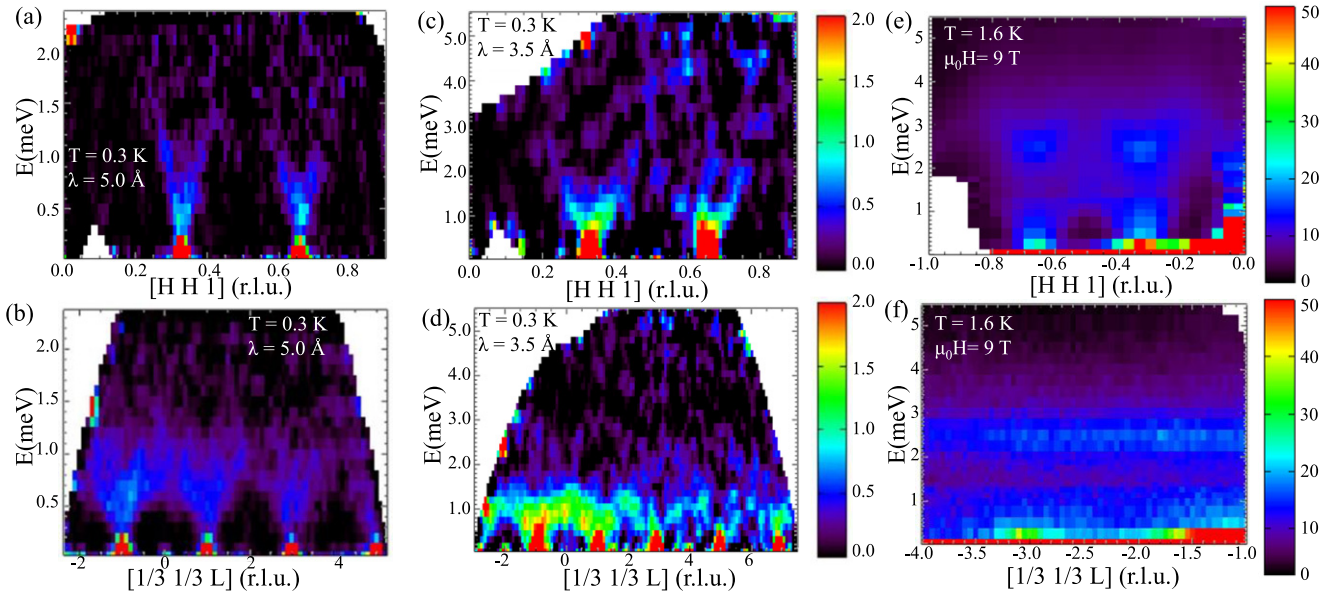

Figure 9. The zero field INS spectra along the [H H 1] (a) and [1/3 1/3 L] (b) directions, which were measured at 300 mK using the wavelength $\lambda = 5$ Å; for (c) and (d), the zero field INS spectra were measured at 300 mK using the wavelength $\lambda = 3.5$ Å. The INS spectra measured at 1.6 K with $H \parallel ab$-plane and $\mu_0 H = 9$ T along [H H 1] (e) and [1/3 1/3 L] (f) directions.

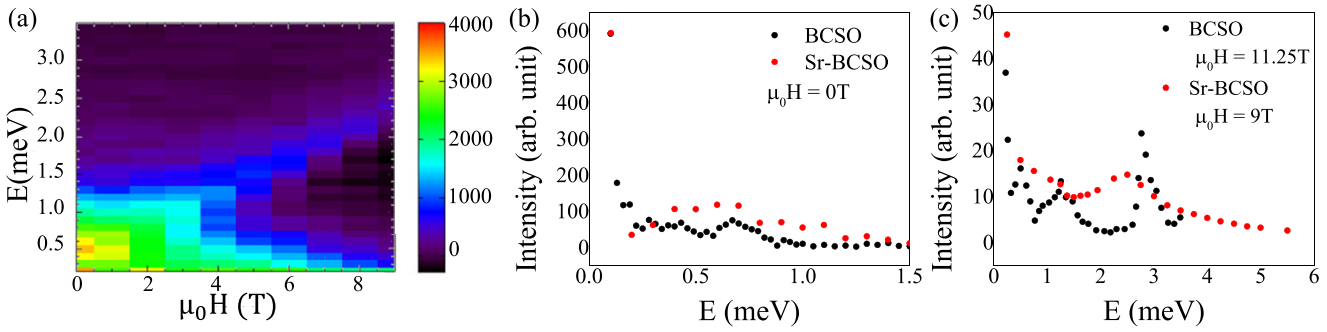

Figure 10. (a) The energy cut at [1/3 1/3 1] as the function of magnetic field with $H \parallel ab$-plane. Comparison of the energy cut between Sr-BCSO and BCSO at the [1/3 1/3 1] position at zero field (b) and applied field (c), which is 9 T for Sr-BCSO and 11.5 T for BCSO.

is quite broad, both of them only show one gapped mode. The energy cut at the zone center of [1/3 1/3 1] plotted in figure 10(b) shows no intensity near zero energy but a broad peak around 0.5 meV, which further confirms that there is only one gapped mode with the gap around 0.5 meV for the INS spectra. Another noteworthy feature is that there is no intensity at the M point for the intralayer dispersion. Figures 9(c) and (d) show the INS spectra up to 5 meV along the two directions, both of them show no obvious intensity at energy above 1.5 meV.

The spectra under 9 T are shown in figures 9(e) and (f) for the two directions, respectively. It is obvious that there are two modes with broad dispersion along the H direction but two flat modes along the L direction. The energy cut at [1/3 1/3 1] plotted in figure 10(c) further confirms that one mode is gapless and the other mode is gapped, with a gap at around 2.5 meV. The more detailed field scan of the cut at [1/3 1/3 1] is shown in figure 10(a). It shows that with increasing field, the gapped mode at zero field splits into two modes, one of which decreases to zero at fields above 6 T while the other mode increases.

4. Discussions

To learn the effects of non-magnetic ion site disorder, we compare several aspects of the observed magnetic properties of Sr-BCSO to those of the parent compound BCSO.

(i) *Anisotropy*. The anomaly at T_{N1} for $\chi(T)$ measured at low fields such as 5 T and the magnetization plateau feature are only observed for $H \parallel ab$-plane in Sr-BCSO. Both features are similar to those of BCSO, which indicates that the Sr-BCSO has the same anisotropy, the easy-plane anisotropy, as BCSO.

(ii) *Magnetic ground state*. The magnetic ground state for Sr-BCSO is a two-step transition with a weak ferromagnetic moment, or a possible canted 120 degree spin structure, as evidenced by the appearance of the [1/3 1/3 0] and [1/3 1/3 2] magnetic peaks at zero field. This is different from that of BCSO, which is a one step transition with a 120 degree spin structure showing no ferromagnetic moment [49, 50, 63].

In BCSO, the [1/3 1/3 0] and [1/3 1/3 2] magnetic peaks only appear under applied fields. The room temperature single crystal diffraction measurement confirms that Sr-BCSO is isostructural to BCSO with an equilateral Co^{2+} triangular layer. The low temperature single crystal neutron diffraction measurements further show no evidence of structural distortion below the magnetic ordering temperatures for Sr-BCSO. Moreover, as argued in (i), both samples have the same easy-plane anisotropy. Therefore, it is surprising to see that the Sr-doping can lead to such a different magnetic ground state in Sr-BCSO.

One possible scenario is that the Sr doping can cause local structural distortion of the CoO_6 octahedra and therefore introduce a spatial anisotropy into the system. This spatial anisotropy, on top of the easy-plane anisotropy, can lead to a two-step transition with canted spins. For example, $Ba_3NiNb_2O_9$ has an equilateral triangular lattice for spin-1 Ni^{2+} ions and orders at 4.9 K with a 120 degree spin structure in the *ab* plane [68]. By replacing Ba^{2+} ion with Ca^{2+} ion with smaller ionic size, a structural distortion is introduced into the system and therefore $Ca_3NiNb_2O_9$ now has a isosceles triangular lattice for Ni^{2+} ions. One consequence is that $Ca_3NiNb_2O_9$ orders with a two-step transition at 4.2 K and 4.8 K [68]. Future studies on the local structure of Sr-BCSO is desirable to exam this possibility and better understand its magnetic ground state.

(iii) *Ordering temperature and ordered moment*. The ordering temperature of Sr-BCSO is around 3.3 K, which is 13% reduction of the ordering temperature, 3.8 K, for BCSO. From the structural view, Sr-BCSO should have higher ordering temperature due to its shorter Co–Co intralayer distance since the Sr doping leads to a smaller lattice parameter *a*, which is 5.847 Å. For BCSO, it is 5.856 Å. Therefore, this lower ordering temperature could be related to the randomization of exchange interactions due to the Ba/Sr mixture. Meanwhile, the ordered moment for Sr-BCSO is around 1.24 μ_B/Co, which is smaller than the 1.5 μ_B/Co of BCSO. For BCSO, we also performed single crystal neutron diffraction measurements and obtained this ordered moment through refinement by using a 120 degree spin structure (the data is not shown here). In fact, both of these ordered moments are smaller than the saturation moment around 1.8 $\sim$ 2 μ_B/Co. In a spin-1/2 triangular lattice antiferromagnet, the reduced ordered moment could be due to the quantum spin fluctuations. Therefore, the even smaller ordered moment of Sr-BCSO indicates that the Sr-doping enhances such kind of spin fluctuations. This enhancement could be another factor for the reduced ordering temperature.

(iv) *Field induced spin state transitions*. For $H \parallel ab$-plane, it is noted that the magnetization at H_{a1} and H_{a2} for Sr-BCSO is 0.5 μ_B and 1.1 μ_B, respectively, which is around 1/3, and $\sqrt{3}/3$ of the saturation value (1.8 μ_B, figure 5(a)). For BCSO, with increasing field along the *ab* plane, its 120 degree spin structure at zero field is followed by a canted 120 degree spin structure, the UUD phase, a coplanar 2:1 canted phase (V phase) with one spin in the 120 degree spin structure rotated to be parallel with another spin, which gives $\sqrt{3}/3M_s$; and another coplanar phase (V′ phase) before entering the fully polarized state [47–50, 53–59]. Therefore, here we tend to assign the phases I, II, and III for $H \parallel ab$-plane of Sr-BCSO as the canted 120 degree spin structure, the UUD phase, and the V phase. For Sr-BCSO, no V′ phase was observed. It is obvious that the magnetization plateau feature in Sr-BCSO is much weaker than that of BCSO, which could be due to the Sr-doping disorder effect. In another triangular lattice antiferromagnet $Rb_{1-x}K_xFe(MoO_4)_2$, the disorder introduced by the K-doping also weakens the magnetization plateau feature related to the UUD phase [76].

As learned from BCSO, while for $H \parallel c$-axis, its 120 degree spin structure will be followed by an umbrella spin structure and a V phase. However, for Sr-BCSO, the magnetic ground state is the canted 120 degree spin structure, which also should be the spin structure for phase I in its $H \parallel c$-axis phase diagram. Therefore, it is difficult to make the analogy between the $H \parallel c$-axis phase diagrams for Sr-BCSO and BCSO. The nature of the phase II for Sr-BCSO needs future studies to clarify.

(v) *Spin dynamics*. The observed INS spectra of Sr-BCSO have several differences from those of BCSO. (a) At zero field, only one gapped mode for Sr-BCSO but two modes (one gapless mode and one gapped mode with gap around 6 $\sim$ 7 meV) for BCSO [61–64]; (b) under field in the UUD phase, two modes for Sr-BCSO but three modes for BCSO [60]. The comparison of the energy cut at the [1/3 1/3 1] position (figures 10(b) and (c)) further highlights these two differences. It is noticed that the two modes at low energy in the UUD phase for BCSO (the data measured at 11.25 T) may merge into each other in the UUD phase for Sr-BCSO (the data measured 9 T), as shown in figure 10(c); (c) no intensity at *M* point for Sr-BCSO but a flat mode and a rotonlike minimum at *M* point for BCSO [61–64]; (d) no intensity above 1.5 meV for Sr-BCSO but a columnar continuum extending to at least 6 meV for BCSO [61–64].

For BCSO, the modes at zero field correspond to the gapless Goldstone mode associated with rotation of the spins in the *ab* plane and an out-of-plane mode that is gapped in the presence of an easy-plane anisotropy, respectively. The rotonlike minimum at *M* point has been related to a magnon decay [63], but is under debate [64]. The origin for the continuum at high energy is not clear so far. As we proposed above, the Sr-doping possibly introduces local spatial anisotropy to account for its two-step magnetic ordering. This spatial anisotropy will break the rotational symmetry of the spins in the *ab* plane. Whether such kind of effect will lead to the disappearance of the gapless mode, or furthermore, the disappearance of the intensity at *M* point and the continuum, needs future theoretical studies to clarify.

In summary, the Sr-doping on the non-magnetic Ba^{2+} ion sites in BCSO affects its magnetic properties profoundly, including the reduction of the ordering temperature and suppression of the magnetization plateau through the randomization of exchange interactions, the reduction of the ordered moment by enhancing quantum spin fluctuations, and the modification of the magnetic ground states, phase diagrams, and spin dynamics by possibly introducing extra spatial anisotropy through local structural distortion. This study serves as a good example for demonstrating that disorder on non-magnetic ion

sites play a complex role on quantum magnetism beyond the expected disruption of the exchange interactions. In fact, such kind of disorder can be treated as an perturbation to efficiently tune the magnetic properties of quantum magnets.

Acknowledgments

QH and HDZ thank the support from NSF-DMR through Award DMR-2003117. A portion of this work was performed at the NHMFL, which is supported by National Science Foundation Cooperative Agreement No. DMR-1157490, the US Department of Energy, and the State of Florida. EF and HBC acknowledge the support of US DOE BES Early Career Award No. KC0402020 under Contract No. DE-AC05-00OR22725. CRW thanks the support from the National Science and Engineering Research Council of Canada (NSERC), and the Canadian Foundation for Innovation (CFI),and the Canada Research Chair programme (Tier II). CM thanks the support from NSERC. WX was supported by Beckman Young Investigator Award. This research used resources at the High Flux Isotope Reactor, a DOE Office of Science User Facility operated by the Oak Ridge National Laboratory. Access to MACS was provided by the Center for High Resolution Neutron Scattering, a partnership between the National Institute of Standards and Technology and the National Science Foundation under Agreement No. DMR-1508249. JM thanks the National Science Foundation of China (No. 11774223 and U2032213). The authors thank Martin Mourigal and his research group for providing help in susceptibility measurements. The identification of any commercial product or trade name does not imply endorsement or recommendation by the National Institute of Standards and Technology.

Data availability statement

The data that support the findings of this study are available upon reasonable request from the authors.

ORCID iDs

Q Huang https://orcid.org/0000-0002-8031-2578
C Mauws https://orcid.org/0000-0003-1826-6432
C R Wiebe https://orcid.org/0000-0002-3681-0182
E X Feng https://orcid.org/0000-0002-3703-1164
H B Cao https://orcid.org/0000-0002-5970-4980

References

[1] Li Y *et al* 2015 *Sci. Rep.* **5** 16419
[2] Li Y, Chen G, Tong W, Pi L, Liu J, Yang Z, Wang X and Zhang Q 2015 *Phys. Rev. Lett.* **115** 167203
[3] Paddison J A, Daum M, Dun Z, Ehlers G, Liu Y, Stone M B, Zhou H and Mourigal M 2017 *Nat. Phys.* **13** 117
[4] Shen Y *et al* 2016 *Nature* **540** 559
[5] Li Y, Adroja D, Voneshen D, Bewley R I, Zhang Q, Tsirlin A A and Gegenwart P 2017 *Nat. Commun.* **8** 15814
[6] Shen Y *et al* 2018 *Nat. Commun.* **9** 4138
[7] Li Y, Adroja D, Biswas P K, Baker P J, Zhang Q, Liu J, Tsirlin A A, Gegenwart P and Zhang Q 2016 *Phys. Rev. Lett.* **117** 097201
[8] Li Y, Bachus S, Liu B, Radelytskyi I, Bertin A, Schneidewind A, Tokiwa Y, Tsirlin A A and Gegenwart P 2019 *Phys. Rev. Lett.* **122** 137201
[9] Xu Y, Zhang J, Li Y, Yu Y, Hong X, Zhang Q and Li S 2016 *Phys. Rev. Lett.* **117** 267202
[10] Ma Z *et al* 2018 *Phys. Rev. Lett.* **120** 087201
[11] Li Y, Adroja D, Bewley R I, Voneshen D, Tsirlin A A, Gegenwart P and Zhang Q 2017 *Phys. Rev. Lett.* **118** 107202
[12] Luo Q, Hu S, Xi B, Zhao J and Wang X 2017 *Phys. Rev.* B **95** 165110
[13] Kimchi I, Nahum A and Senthil T 2018 *Phys. Rev.* X **8** 031028
[14] Parker E and Balents L 2018 *Phys. Rev.* B **97** 184413
[15] Kawamura H and Uematsu K 2019 *J. Phys.: Condens. Matter.* **31** 504003
[16] Zhu Z, Maksimov P, White S R and Chernyshev A 2017 *Phys. Rev. Lett.* **119** 157201
[17] Zhu Z, Maksimov P, White S R and Chernyshev A 2018 *Phys. Rev. Lett.* **120** 207203
[18] Wu H-Q, Gong S-S and Sheng D 2019 *Phys. Rev.* B **99** 085141
[19] Kaneko R, Morita S and Imada M 2014 *J. Phys. Soc. Japan* **83** 093707
[20] Li P H, Bishop R F and Campbell C E 2015 *Phys. Rev.* B **91** 014426
[21] Zhu Z and White S R 2015 *Phys. Rev.* B **92** 041105
[22] Hu W-J, Gong S-S, Zhu W and Sheng D 2015 *Phys. Rev.* B **92** 140403
[23] Iqbal Y, Hu W-J, Thomale R, Poilblanc D and Becca F 2016 *Phys. Rev.* B **93** 144411
[24] Saadatmand S and McCulloch I 2016 *Phys. Rev.* B **94** 121111
[25] Kimchi I, Sheckelton J P, McQueen T M and Lee P A 2018 *Nat. Commun.* **9** 4367
[26] Volkov P A, Won C-J, Gorbunov D, Kim J, Ye M, Kim H-S, Pixley J, Cheong S-W and Blumberg G 2020 *Phys. Rev.* B **101** 020406
[27] Kundu S *et al* 2020 *Phys. Rev. Lett.* **125** 117206
[28] Song P *et al* 2021 arXiv:2103.05820
[29] Syzranov S and Ramirez A 2021 arXiv:2105.08070
[30] Liu L, Shao H, Lin Y-C, Guo W and Sandvik A W 2018 *Phys. Rev.* X **8** 041040
[31] Hong W *et al* 2021 *Phys. Rev. Lett.* **126** 037201
[32] Baek S-H, Yeo H W, Do S-H, Choi K-Y, Janssen L, Vojta M and Büchner B 2020 *Phys. Rev.* B **102** 094407
[33] Do S-H *et al* 2020 *Phys. Rev. Lett.* **124** 047204
[34] Huang Y *et al* 2021 arXiv:2105.14749
[35] Hu X *et al* 2021 *Phys. Rev. Lett.* **127** 017201
[36] Ren H-D, Xiong T-Y, Wu H-Q, Sheng D and Gong S-S 2020 arXiv:2004.02128
[37] Gomez S *et al* 2021 *Phys. Rev.* B **103** 214419
[38] Shimokawa T, Watanabe K and Kawamura H 2015 *Phys. Rev.* B **92** 134407
[39] Kawamura H, Watanabe K and Shimokawa T 2014 *J. Phys. Soc. Japan* **83** 103704
[40] Watanabe K, Kawamura H, Nakano H and Sakai T 2014 *J. Phys. Soc. Japan* **83** 034714
[41] Uematsu K and Kawamura H 2017 *J. Phys. Soc. Japan* **86** 044704
[42] Uematsu K and Kawamura H 2018 *Phys. Rev.* B **98** 134427
[43] Uematsu K and Kawamura H 2019 *Phys. Rev. Lett.* **123** 087201
[44] Rao X *et al* 2021 *Nat. Commun.* **12** 4949
[45] Miyashita S 1986 *J. Phys. Soc. Japan* **55** 3605
[46] Chubukov A and Golosov D 1991 *J. Phys.: Condens. Matter.* **3** 69
[47] Shirata Y, Tanaka H, Matsuo A and Kindo K 2012 *Phys. Rev. Lett.* **108** 057205

[48] Susuki T, Kurita N, Tanaka T, Nojiri H, Matsuo A, Kindo K and Tanaka H 2013 *Phys. Rev. Lett.* **110** 267201
[49] Sera A, Kousaka Y, Akimitsu J, Sera M, Kawamata T, Koike Y and Inoue K 2016 *Phys. Rev.* B **94** 214408
[50] Zhou H *et al* 2012 *Phys. Rev. Lett.* **109** 267206
[51] Li M, Zelenskiy A, Quilliam J, Dun Z, Zhou H, Plumer M and Quirion G 2019 *Phys. Rev.* B **99** 094408
[52] Quirion G, Lapointe-Major M, Poirier M, Quilliam J, Dun Z and Zhou H 2015 *Phys. Rev.* B **92** 014414
[53] Gekht R S and Bondarenko I N 1997 *J. Exp. Theor. Phys.* **84** 345
[54] Chen R, Ju H, Jiang H-C, Starykh O A and Balents L 2013 *Phys. Rev.* B **87** 165123
[55] Starykh O A, Jin W and Chubukov A V 2014 *Phys. Rev. Lett.* **113** 087204
[56] Yamamoto D, Marmorini G and Danshita I 2014 *Phys. Rev. Lett.* **112** 127203
[57] Koutroulakis G, Zhou T, Kamiya Y, Thompson J, Zhou H, Batista C and Brown S 2015 *Phys. Rev.* B **91** 024410
[58] Yamamoto D, Marmorini G and Danshita I 2015 *Phys. Rev. Lett.* **114** 027201
[59] Liu X, Prokhnenko O, Yamamoto D, Bartkowiak M, Kurita N and Tanaka H 2019 *Phys. Rev.* B **100** 094436
[60] Kamiya Y *et al* 2018 *Nat. Commun.* **9** 3110
[61] Ito S, Kurita N, Tanaka H, Ohira-Kawamura S, Nakajima K, Itoh S, Kuwahara K and Kakurai K 2017 *Nat. Commun.* **8** 235
[62] Verresen R, Moessner R and Pollmann F 2019 *Nat. Phys.* **15** 750
[63] Ma J *et al* 2016 *Phys. Rev. Lett.* **116** 087201
[64] Macdougal D, Williams S, Prabhakaran D, Bewley R I, Voneshen D J and Coldea R 2020 *Phys. Rev.* B **102** 064421
[65] Mourigal M, Fuhrman W, Chernyshev A and Zhitomirsky M 2013 *Phys. Rev.* B **88** 094407
[66] Ghioldi E A, Mezio A, Manuel L O, Singh R, Oitmaa J and Trumper A E 2015 *Phys. Rev.* B **91** 134423
[67] Maksimov P, Zhitomirsky M and Chernyshev A 2016 *Phys. Rev.* B **94** 140407
[68] Lu Z, Ge L, Wang G, Russina M, Günther G, dela Cruz C, Sinclair R, Zhou H and Ma J 2018 *Phys. Rev.* B **98** 094412
[69] Primo-Martín V and Jansen M 2001 *J. Solid State Chem.* **157** 76
[70] Lee M, Hwang J, Choi E, Ma J, Cruz C D, Zhu M, Ke X, Dun Z and Zhou H 2014 *Phys. Rev.* B **89** 104420
[71] Lee M, Choi E, Ma J, Sinclair R, Cruz C D and Zhou H 2017 *Mater. Res. Bull.* **88** 308
[72] Yokota K, Kurita N and Tanaka H 2014 *Phys. Rev.* B **90** 014403
[73] Sheldrick G M 2015 *Acta Crystallogr.* C **71** 3
[74] Cao H *et al* 2019 *Crystals* **9** 5
[75] Rodriguez J *et al* 2008 *Meas. Sci. Technol.* **19** 034023
[76] Smirnov A, Soldatov T, Petrenko O, Takata A, Kida T, Hagiwara M, Shapiro A Y and Zhitomirsky M 2017 *Phys. Rev. Lett.* **119** 047204